Geoderma 429 (2023) 116263

Contents lists available at ScienceDirect

Geoderma

journal homepage: www.elsevier.com/locate/geoderma

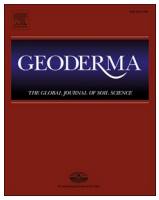

A four-parameter-based thermo-TDR approach to estimate water and NAPL contents of soil liquid

Yuki Kojima [a,*], Kenta Okumura [b], Shinsuke Aoki [c], Kosuke Noborio [d], Kohji Kamiya [a], Robert Horton [e]

[a] Department of Civil Engineering, Gifu University, 1-1 Yanagido, Gifu City, Gifu 501-1193, Japan
[b] Graduate School of Natural Science and Technology, Gifu University, 1-1 Yanagido, Gifu City, Gifu 501-1193, Japan
[c] National Institute of Advanced Industrial Science and Technology, Tsukuba Central 7, 1-1-1 Higashi, Tsukuba, Ibaraki 305-8567, Japan
[d] School of Agriculture, Meiji University, 1-1-1 Higashimita, Tama-Ku, Kawasaki City, Kanagawa 214-8571, Japan
[e] Department of Agronomy, Iowa State University, Ames, IA 50011, USA

ARTICLE INFO

Handling Editor: Morgan Cristine L.S.

Keywords:
Soil non-aqueous phase liquid contamination
Thermo-time domain reflectometry
Soil electrical properties
Soil thermal properties
Sensitivity analysis

ABSTRACT

In-situ determination of soil non-aqueous phase liquid content (θ_{NAPL}) is necessary for early detection of soil NAPL contamination and preventing the spread of the contamination. Thermo-time domain reflectometry (thermo-TDR), which can simultaneously measure dielectric constant, electrical conductivity, volumetric heat capacity, and thermal conductivity, has the potential to estimate θ_{NAPL}. The objectives of the study are i) to establish a relationship between the four thermo-TDR measured soil properties and soil water content (θ_w) and θ_{NAPL} values and ii) to evaluate the sensitivities of the thermo-TDR measured properties to θ_w and θ_{NAPL}, and iii) to develop a four-parameter based approach to simultaneously determine θ_w and θ_{NAPL}. Thermo-TDR measurements were performed on sand and glass beads containing various amounts of water and Canola oil as a NAPL. In all cases θ_w rather than θ_{NAPL} dominated all four thermo-TDR measured properties. A sensitivity analysis also indicated that all four properties were more sensitive to θ_w than to θ_{NAPL}. Among the four properties, the dielectric constant, electrical conductivity, and volumetric heat capacity were somewhat sensitive to θ_{NAPL}, while thermal conductivity was not sensitive. A new approach using all four thermo-TDR measured properties (four-parameter-based approach) to estimate θ_{NAPL} was found to be more accurate than the existing two property-based approaches, i.e., dielectric constant and volumetric heat capacity-based. The root mean square error (RMSE) values for θ_{NAPL} estimation with the four-parameter-based approach were 0.066 and 0.042 $m^3\ m^{-3}$ for sand and glass beads, while the two property-based approach had RMSE values of 0.180 and 0.220 $m^3\ m^{-3}$. The four-parameter-based approach enabled suppression of the effects of measurement errors by the optimization processes and allowed the high sensitivity parameters to cover for shortcomings in the low sensitivity parameters. Use of thermo-TDR sensors with the four-parameter-based approach to determine θ_{NAPL} can contribute to various NAPL soil contamination studies as a NAPL content quantifying approach.

1. Introduction

In recent years, soil contamination with non-aqueous phase liquid (NAPL), including oils and volatile organic compounds, has been a critical environmental issue (Soga et al., 2004). A portion of a NAPL added to soil can move in the unsaturated zone in both liquid and gas phases and eventually reach the groundwater table (Leharne, 2019). Once a NAPL reaches the groundwater table, it can be transported horizontally with the groundwater flow (McCray and Falta, 1997). Given that, NAPL contamination in groundwater tends to spread widely. Therefore, early detection of NAPL contamination is essential, and in-situ determination of soil NAPL content (θ_{NAPL}) is valuable information.

The θ_{NAPL} of soils saturated with liquid (water and NAPL) can be determined accurately with dielectric constant measurements (Rinaldi

Abbreviations: NAPL, non-aqueous phase liquid; DPHP, dual probe heat pulse; TDR, time domain reflectometry; RMSE, root mean squared error; MAPE, mean absolute percentage error.

* Corresponding author.
E-mail addresses: kojima@gifu-u.ac.jp (Y. Kojima), shinsuke-aoki@aist.go.jp (S. Aoki), noboriok@meiji.ac.jp (K. Noborio), kkamiya@gifu-u.ac.jp (K. Kamiya), rhorton@iastate.edu (R. Horton).

https://doi.org/10.1016/j.geoderma.2022.116263
Received 21 April 2022; Received in revised form 23 August 2022; Accepted 10 November 2022
Available online 25 November 2022

and Francisca, 2006; Moroizumi and Sasaki, 2008; Francisca and Montoro, 2012). Researchers have attempted to quantify in-situ θ_{NAPL} based on either soil electrical or thermal properties. Time domain reflectometry (TDR) is a widely used technique to determine soil bulk dielectric constant (ε_b) (Topp et al., 1980; Noborio, 2001), and it has been used for θ_{NAPL} determination (Ajo-Franklin et al., 2004; Mohanmed and Said, 2004, 2005). The ε_b measurement with TDR was utilized to detect a front of NAPL infiltration (Comegna et al., 2018) and decontamination process of NAPL with soil flushing (Comegna et al., 2019). While some researchers used ε_b measurements to estimate θ_{NAPL}, Moroizumi et al. (2008) used a dual probe heat pulse (DPHP) technique (Campbell et al., 1991; Bristrow et al., 1994) to measure soil volumetric heat capacity (C) and convert it to θ_{NAPL} with empirically obtained models. Their approach showed that θ_{NAPL} of liquid saturated soil could be estimated accurately.

While θ_{NAPL} in saturated soil was successfully determined, its quantification in unsaturated soil has been elusive. Persson and Berndtsson (2002) used TDR measured ε_b and soil bulk electrical conductivity (σ_b) values to determine volumetric water content (θ_w) and θ_{NAPL} in variably saturated soil. Although their approach determined θ_w and θ_{NAPL} accurately, its applicability was restricted because of the complicated procedures, extensive detailed data set necessary for calibration, and sensitivity of σ_b to non-uniform distribution of water and NAPL. Haridy et al. (2004) reported that the Persson and Berndtsson (2002) approach did not accurately determine θ_{NAPL} of fine sand. They examined a similar empirical approach for fine sand, but its applicability was restricted to relatively small θ_{NAPL} values. Comegna et al. (2016) developed an improved approach to determine θ_{NAPL} from ε_b and σ_b with a more general calibration procedure. As an alternative method for quantifying θ_{NAPL} in unsaturated soils, Noborio (2005) proposed using thermo-time domain reflectometry (thermo-TDR). A thermo-TDR sensor combines TDR and DPHP methods (Noborio et al., 1996; Ren et al., 1999) to measure two soil electrical properties, ε_b and σ_b, and two thermal properties, C and thermal conductivity (λ). Noborio (2005) reported that a combination of C and σ_b could determine θ_{NAPL}. Aoki and Noborio (2019) and Ju et al. (2020) used a thermo-TDR sensor to determine θ_w and θ_{NAPL} simultaneously in variably saturated soil. They developed an empirical expression of θ_{NAPL} as a function of C and ε_b, which provided relatively accurate determinations of θ_w and θ_{NAPL}. So far, studies using thermo-TDR measurements to determine θ_{NAPL} have involved only two of the four soil properties that a thermo-TDR sensor can measure. Using only two properties is feasible because knowledge of only two of the four properties is required in order to estimate the two unknown parameters, i.e., θ_w and θ_{NAPL}. However, a possibility exists that the performance of thermo-TDR based θ_{NAPL} estimations can be improved by utilizing all four properties, i.e. ε_b, σ_b, C, and λ. For this purpose, it is vital to understand the effect of θ_w and θ_{NAPL} on each soil property.

Therefore, the objectives of this study are as follows: i) to perform thermo-TDR measurements in soils having various θ_w and θ_{NAPL} values and express the relationships with adequate models, ii) to evaluate the sensitivity of ε_b, σ_b, C, and λ to θ_w and θ_{NAPL}, and iii) to develop a four-parameter based approach to simultaneously determine θ_w and θ_{NAPL}.

2. Materials and methods

2.1. Thermo-time domain reflectometry theory

The thermo-TDR sensor designed by Ren et al. (1999) was used in this study. The sensor consists of three 40 mm stainless steel tubes with 0.9 mm and 1.3 mm inner and outer diameters. Tube spacing distance is about 6 mm. A 75 Ω coaxial cable is soldered to one end of each stainless steel tube to propagate the pulsed electromagnetic signal. The center tube embeds a resistance heater wire and a type T thermocouple, and the two outside tubes embed a type T thermocouple. The resistance heater wire is doubled over twice and produces a heater resistance of 533 Ω m^{-1}. The thermocouples inside stainless steel tubes are located 20 mm away from the tip of the tubes. The thermo-TDR measures ε_b from the time that it takes for an electromagnetic signal to propagate along the tubes (Noborio, 2001):

$$\varepsilon_b = \left(\frac{ct}{2L}\right)^2 \tag{1}$$

where c is the velocity of an electromagnetic wave in free space (3×10^8 m s^{-1}), t is the round-trip time (s), and L is the probe length of the thermo-TDR tubes (m). The σ_b (mS m^{-1}) is determined from the amplitude of the reflected signal as follows (Noborio, 2001):

$$\sigma_b = \left(\frac{K}{Z_u}\right)\left(\frac{1-\rho_\infty}{1+\rho_\infty}\right) \tag{2}$$

where K is the geometric constant of a probe (m^{-1}) determined by calibrations with known electrical conductivity solutions, Z_u is the cable impedance (Ω), and ρ_∞ is the reflection coefficient at a distant point from the first reflection point on the waveform. The reflection coefficient is the ratio of the amplitude of the reflected signal to that of the applied signal. Details of the TDR function can be found in Noborio (2001) and Robinson et al. (2002).

The DPHP function of the thermo-TDR sensor can be used to determine C (J m^{-3} °C^{-1}) and λ (W m^{-1} °C^{-1}) from the temperature response of the outer tubes to a heat input applied via the heater wire in the center tube. The temperature change ΔT (°C) at the outer tubes is described as (Bristrow et al., 1994):

$$\Delta T = \begin{cases} -\dfrac{q'}{4\pi\lambda}\mathrm{Ei}\left(\dfrac{-r^2C}{4\lambda t}\right) & 0 < t \leqslant t_0 \\ \dfrac{q'}{4\pi\lambda}\left[\mathrm{Ei}\left(\dfrac{-r^2C}{4\lambda(t-t_0)}\right) - \mathrm{Ei}\left(\dfrac{-r^2C}{4\lambda t}\right)\right] & t > t_0 \end{cases} \tag{3}$$

where q' is heat flux applied at the center tube (W m^{-1}), r is the distance of the side tube from the center tube (m), t is time (s), t_0 is the heating duration (s), and Ei is the exponential integral. Eq. (3) is fitted to temperature change with time observations to find the best combination of C and λ. A detailed review of the DPHP method is provided by He et al. (2018).

2.2. Thermo-time domain reflectometry measurements

Thermo-TDR measurements were performed on Toyoura sand and on glass beads (ASGB-320, AS ONE, Osaka, Japan). Both Toyoura sand and glass beads have relatively homogeneous particle sizes. The Toyoura sand particles had diameters ranging from 0.10 to 0.25 mm, while the glass beads diameters ranged from 0.025 to 0.075 mm. This study used Canola oil (density of $\rho_o = 920$ kg m^{-3}) as the NAPL, because it was safe to handle and had small volatility. Mixtures of water and Canola oil were added to sand and glass bead samples to produce various θ_w and θ_{NAPL} values. The materials and water-NAPL liquids were mixed well in plastic bags by shaking and with crashed aggregates, and stored over night. Each sample mixture was packed into a 5 cm inner diameter and 5 cm tall plastic ring at known bulk density (sand: 1,350 kg m^{-3} and glass beads: 1,400 kg m^{-3}). The volumetric content of the mixed liquids in the samples, i.e., liquid content ($\theta_l = \theta_w + \theta_{NAPL}$), was controlled to be 0.05, 0.10, 0.15, 0.20, and 0.30 m^3 m^{-3}. The liquid mixture volumetric ratios of water and NAPL were 100 to 0, 75 to 25, 50 to 50, 25 to 75, and 0 to 100, i.e., concentrations of NAPL in liquid were 0, 25, 50, 75, and 100 %, respectively. A thermo-TDR sensor was inserted vertically into each packed sample and used to measure electrical and thermal properties. A datalogger CR1000 (Campbell Scientific, Logan, UT) and time domain reflectometer TDR200 (Campbell Scientific) were used for data acquisition. For the DPHP measurements, a 70 W m^{-1} heat intensity was applied for 8 s, and associated temperature changes were recorded each second for 180 s. Eq. (3) was fitted to the entire 180-point temperature change dataset. The measurements were repeated three times with a 30

min interval. Three samples were prepared for each combination of θ_w and θ_{NAPL}. Two of the samples were used to develop models of the soil electrical and thermal properties as functions of θ_w and θ_{NAPL} described in 2.3, and the other sample was used to validate the approaches to determine θ_w and θ_{NAPL} described in 2.5.

2.3. Model evaluation of the four soil properties

The relationships obtained between θ_l and each soil property were expressed with models that considered the effects of the NAPL. A dielectric mixing model which expressed ε_b as a function of volume fraction and dielectric constant of each soil constituent was used when the sample contained water and NAPL (e.g., Persson and Berndtsson, 2002; Comegna et al., 2016):

$$\varepsilon_b{}^{\alpha} = \theta_s\varepsilon_s{}^{\alpha} + \theta_w\varepsilon_w{}^{\alpha} + \theta_{NAPL}\varepsilon_{NAPL}{}^{\alpha} + \theta_a\varepsilon_a{}^{\alpha} \quad (4)$$

where θ and ε are volume fraction and dielectric constant of soil constituents, and α is an empirical parameter for soil geometry. The subscripts s, w, NAPL and a representative solids, water, NAPL and air, respectively. The values of ε_w and ε_{NAPL} were taken from the literature as 80 and 3.1, respectively (Lizhi et al., 2008). The value of α depended on the geometry of the soil constituents, and it varied with soil and liquid type. Although Birchak et al. (1974) proposed using a constant value of 0.5, α is often treated as a fitting parameter when matching Eq. (4) to observations (Regalado et al., 2003). Persson and Berndtsson (2002) used α as a function of θ_{NAPL} to obtain an accurate fit of Eq. (4) to the observations. However, this approach required detailed calibration data which complicated the θ_w and θ_{NAPL} estimation procedure. Values of ε_s are reported in the literature for specific compositions of soil particles, but the actual values are unknown for most soils. Therefore, we used α and ε_s as constant fitting parameters in this study. The σ_b values were determined by the Rhoades et al. (1976) relationship:

$$\sigma_b = \sigma_w\theta_w T(\theta_w) + \sigma_s \quad (5)$$

where σ_w and σ_s are the electrical conductivities of soil water and soil matrix surface (mS m^{-1}), $T(\theta_w)$ is the tortuosity coefficient for electrical current flow. $T(\theta_w)$ is treated as a linear function of θ_w as $T(\theta_w) = a\theta_w + b$. Because Eq. (5) does not include terms associated with θ_{NAPL}, Persson and Berndtsson (2002) make σ_s, and the empirical parameters a and b vary with a change in θ_{NAPL}. This procedure complicates the calibration process. In this study, we incorporate new terms associated with θ_{NAPL} into Eq. (5) as follows:

$$\sigma_b = \sigma_w\theta_w T(\theta_w) + \sigma_{NAPL}\theta_{NAPL} T(\theta_{NAPL}) + \sigma_s \quad (6)$$

where σ_{NAPL} is the electrical conductivity of NAPL, $T(\theta_{NAPL})$ is the tortuosity coefficient for electrical current flow affected by the presence of NAPL. Although NAPL is an insulating material, e.g., electrical conductivity of Canola oil is smaller than 5.0 $\times$ 10^{-6} mS m^{-1} (Sankaran et al., 2019), we assume it somewhat affects the electrical current pathway by influencing water distribution and soil particle connectivity. We treat $T(\theta_{NAPL})$ as a linear function of θ_{NAPL} as $T(\theta_{NAPL}) = d\theta_{NAPL} + e$ similar to $T(\theta_w)$. The σ_w value is set at 242 mS m^{-1} (Persson and Berndtsson, 2002), and σ_{NAPL}, σ_s, and empirical parameters a, b, d, and e are determined by data fitting.

The C is described as the sum of the products of the volume fraction and volumetric heat capacity of each soil constituent (de Vries, 1963):

$$C = \theta_s C_s + \theta_w C_w + \theta_{NAPL} C_{NAPL} + \theta_a C_a \quad (7)$$

where C_s, C_w, C_{NAPL}, and C_a are volumetric heat capacities (J m^{-3} °C^{-1}) of soil solid, water, NAPL, and air. The values of C_w and C_{NAPL} are 4.18 $\times$ 10^6 J m^{-3} °C^{-1} and 1.69 $\times$ 10^6 J m^{-3} °C^{-1} at 20 °C (de Vries, 1963; Rojas et al., 2013). The fourth term, $\theta_a C_a$, is often ignored because the C_a is smaller than those of other soil constituents. The $\theta_s C_s$ value depends on soil materials and bulk density, and in this study, we determine it by data fitting. Mochizuki et al. (2007) calculate λ of NAPL contaminated soil based on θ_w, θ_{NAPL}, and thermal conductivities of soil containing either water or NAPL only (λ_w and λ_{NAPL}). We incorporate weighting factors, w_1 and w_2, to express the relationship more accurately:

$$\lambda = \frac{w_1\theta_w\lambda_w + w_2\theta_{NAPL}\lambda_{NAPL}}{w_1\theta_w + w_2\theta_{NAPL}} \quad (8)$$

It is necessary to model the λ_w and λ_{NAPL} as a function of θ_l where $\theta_l = \theta_w$ for λ_w and $\theta_l = \theta_{NAPL}$ for λ_{NAPL} to use Eq. (8). We use an expression similar to the model proposed by Lu et al. (2014):

$$\lambda_w = \lambda_{dry} + \exp\left(\gamma_1 - \theta_l{}^{-\beta_1}\right)$$

$$\lambda_{NAPL} = \lambda_{dry} + \exp\left(\gamma_2 - \theta_l{}^{-\beta_2}\right) \quad (9)$$

where λ_{dry} is the thermal conductivity of an oven-dried soil (W m^{-1} °C^{-1}), β_1, β_2, γ_1, and γ_2 are empirical parameters associated with soil type. While Lu et al. (2014) provide equations to predict λ_{dry}, β, and γ from soil texture and bulk density, we determine them by fitting Eq. (9) to the thermal conductivity observations with soils containing only water or NAPL. After the determination of empirical parameters in Eq. (9), w_1 and w_2 in Eq. (8) are determined by fitting Eq. (8) to the thermal conductivities of soils containing both water and NAPL. The model performance is evaluated with the root mean squared errors (RMSE) and the mean absolute percentage error (MAPE) (Yilmaz and Kaynar, 2011):

$$\mathrm{RMSE} = \sqrt{\frac{\sum\left[X_{observ} - X_{model}\right]^2}{n}} \quad (10)$$

$$\mathrm{MAPE} = \frac{1}{n}\sum\left|\frac{X_{observ} - X_{model}}{x_{observ}}\right| \times 100 \quad (11)$$

where X is the electrical or thermal properties, the subscript *observ* and *model* represent the values measured with thermo-TDR and the modeled values. The influence of NAPL on soil electrical and thermal properties is discussed based on these models.

2.4. Sensitivity analysis

The sensitivity of each soil property to changes in θ_w and θ_{NAPL} was evaluated. The sensitivity analysis procedure followed Kojima et al. (2018) with the models for each property shown in 2.3. The θ_w and θ_{NAPL} values were set from 0 m^3 m^{-3} to 0.50 m^3 m^{-3} with increments of 0.1 m^3 m^{-3}. The cases for which the total of θ_w and θ_{NAPL}, i.e., θ_l, was larger than porosity (0.50 m^3 m^{-3}) were eliminated, and 21 cases were tested. In each case, a $\pm$ 1 % error was incorporated into θ_w and θ_{NAPL}, and the change in each property was calculated. The sensitivity coefficients were calculated with the following equation (Kojima et al., 2018):

$$\varphi = \frac{\partial y}{\partial x}\frac{x}{y} \quad (12)$$

where y represents electrical or thermal properties, and x represents θ_w or θ_{NAPL}. The values of φ were used to identify which properties were significantly affected by changes in θ_w and θ_{NAPL}.

2.5. Determination of water and non-aqueous phase liquid contents

The determination of θ_w and θ_{NAPL} is performed via three different approaches. The first approach is based on the values of ε and C, which is similar to Noborio (2013) and Ju et al. (2020). Eq. (13), which determines θ_w from ε and C values, can be derived by combining Eqs. (4) and (7):

$$\theta_w = \frac{C_{NAPL}(\varepsilon_b{}^{\alpha} - \varepsilon_a{}^{\alpha}) - C_{NAPL}\theta_s(\varepsilon_s{}^{\alpha} - \varepsilon_a{}^{\alpha}) - (C - C_s)(\varepsilon_{NAPL}{}^{\alpha} - \varepsilon_a{}^{\alpha})}{C_{NAPL}(\varepsilon_w{}^{\alpha} - \varepsilon_a{}^{\alpha}) - C_w(\varepsilon_{NAPL}{}^{\alpha} - \varepsilon_a{}^{\alpha})} \quad (13)$$

Once θ_w is determined with Eq. (13), θ_{NAPL} can be determined with Eq. (7).

The second approach is based on ε and λ values. While determinations of C are affected by the deflection of probe spacing, which can occur when a sensor is inserted into a soil, the determination of λ is independent of the probe spacing. Therefore, we examine the use of ε and λ to determine θ_w and θ_{NAPL}. Equations (4) and (8) are relatively complicated, and it is not easy to derive a simple form to determine θ_w and θ_{NAPL}. Thus, we determine the best combination of θ_w and θ_{NAPL} by optimization to minimize the absolute relative errors between the measured values and the estimated values for both ε_b and λ.

The third approach uses all four thermo-TDR measured parameters. The best combination of θ_w and θ_{NAPL} that yields the smallest total absolute error between the measured and estimated values is found by optimization. The total absolute relative error δ_t is calculated as follows:

$$\delta_t = \left|\frac{\varepsilon_{b,\ observ} - \varepsilon_{b,model}}{\varepsilon_{b,observ}}\right| + \left|\frac{\sigma_{b,\ observ} - \sigma_{b,model}}{\sigma_{b,observ}}\right| + \left|\frac{C_{observ} - C_{model}}{C_{observ}}\right| + \left|\frac{\lambda_{observ} - \lambda_{model}}{\lambda_{observ}}\right| \quad (14)$$

The initial estimate of θ_w and θ_{NAPL} for this optimization with Eq. (14) must be carefully determined to avoid falling into local minima, which may result in inaccurate estimation of θ_w and θ_{NAPL}. In this study, we use θ_w calculated with Eq. (13) for initial estimates of θ_w and perform a two-step optimization process. We first optimize only θ_{NAPL} with a 0.1 $m^3\ m^{-3}$ as an initial estimate. After that, the second optimization of both θ_w and θ_{NAPL} is performed using the θ_{NAPL} values from the first optimization as an initial value. The Microsoft Exel Solver function is used to perform the optimization.

The θ_w and θ_{NAPL} values determined with each approach are compared with reference values, which are known when preparing the samples, and its estimation performances are evaluated with RMSE values calculated with Eq. (10) where the soil property X is replaced by θ_w and θ_{NAPL}.

3. Results and discussion

3.1. Effects of soil water and NAPL contents on soil properties

Fig. 1 presents various relationships between ε_b and θ_l for the sand and the glass beads. The effects of various NAPL concentrations on ε_b are shown as different color plots. The ε_b values increased as θ_l increased, but the increase rate depended on NAPL concentration in the liquid. The lower the concentration of NAPL in the solution (the larger the percentage of water), the larger the increase in ε_b, and conversely, the higher the concentration of NAPL, the smaller the increase. For example, while the ε_b value increased by 16.4 as θ_l increased from 0.05 $m^3\ m^{-3}$ to 0.30 $m^3\ m^{-3}$ for 0 % NAPL concentration, the ε_b increase was only 1.0 for 100 % NAPL. Compared to sand, glass beads have slightly larger ε_b values over the entire range of θ_w and θ_{NAPL}. These trends occur because NAPL has a smaller ε value than does water. The θ_w dominates the ε_b, and the effect of NAPL contamination is relatively small. The fitting results of Eq. (4) are also shown as solid lines in Fig. 1. The obtained fitting parameters are shown in Table 1. Eq. (4) expresses the relationship between θ_w, θ_{NAPL}, and ε_b well for both sand and glass beads. The RMSE values are 0.59 for sand and 0.51 for glass beads, and the MAPE values are 7.6 % for sand and 5.3 % for glass beads. The glass beads experience slightly better fits due to smaller measurement errors in ε_b. The estimated values of ε_s and α are reasonable. The ε_s of sand is 3.69, which is close to the ε of quartz, 3.8, and that of glass beads is 7.51, which is within the range of reported ε values for various glass materials, from 3.8 to 9.5 (Frederikse, 2009). The α values are similar to values reported in earlier studies, e.g., 0.5 by Birchak et al. (1974) and 0.65 by Dobson et al. (1985). This implies that the NAPL intrusion does not influence the geometry of soil constituents.

The relationship between θ_l and σ_b is presented in Fig. 2. The σ_b values increased as θ_l increased. The rate of increase was greater when the concentration of NAPL in the solution was low. When θ_l increased from 0.05 $m^3\ m^{-3}$ to 0.30 $m^3\ m^{-3}$, the increase in σ_b of the sand was 3.4 mS m^{-1} and 0.6 mS m^{-1} for 0 % and 100 % NAPL concentration, while for the glass beads the increases in σ_b were 19.9 mS m^{-1} and 0.3 mS m^{-1}. Only slight increases in the σ_b value occurred when NAPL concentration was 100 %. This indicated that the NAPL had a negligible effect on σ_b and that σ_b wasmainly governed by θ_w. The slight increase might be associated with the increased electrical pathway associated with NAPL connecting the soil particles. Thus, as we assumed in Eq. (6), NAPL affected σ_b even though it had a small electrical conductivity. The σ_b values of glass beads were approximately-three times larger than those for sand. This could be due to the smaller pore size and more sparse water distribution in the glass beads, resulting in a more diverse transfer pathway. Looking at the fitting results of Eq. (6) (solid lines in Fig. 2 and fitting parameters are shown in Table 1), the relationship between θ_l and σ_b can be expressed relatively accurately. However, when compared to ε_b, some measured σ_b values are noticeably different from the model. This implies that σ_b is susceptible to minor variations in θ_w, temperature, and bulk density, and that measurement errors may be significant.

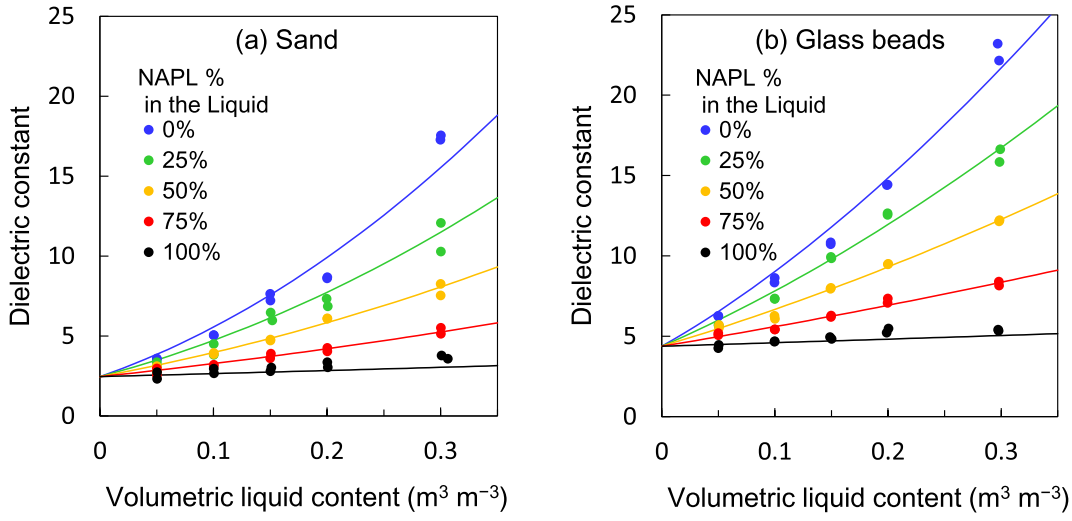

Fig. 1. The relationship between soil volumetric liquid content and bulk dielectric constant. Points are the observations and solid curves are fits of Eq. (4) to data. Different colors represent different concentrations of non-aqueous phase liquid (NAPL) in the soil liquid.

Table 1
Parameters obtained by fitting models to measured values. Dielectric constant of soil particles (ε_s) and soil geometry factor (α) for Eq. (4), electrical conductivity of soil particles and non-aqueous phase liquid (NAPL) (σ_s and σ_{NAPL}) and tortuosity parameters (a, b, d, e) for Eq. (6), volumetric heat capacity of dry soil ($\theta_s C_s$) for Eq. (7), and weighting factors (w_1 and w_2), thermal conductivities of dry materials (λ_{dry}), and shape factors (β_1, β_2, γ_1, and γ_2) for Eqs. (8, 9).

Material	Dielectric constant		Electrical conductivity					
	ε_s	α	σ_s (mS m^{-1})	σ_{NAPL} (mS m^{-1})	a	b	d	e
Sand	3.69	0.54	3.47	1.28	0.102	0.013	0.004	1.097
Glass beads	7.51	0.68	4.16	2.01	0.336	0.152	0	2.494

Material	Volumetric heat capacity	Thermal conductivity						
	$\theta_s C_s$ (J m^{-3} °C^{-1})	w_1	w_2	λ_{dry} (W m^{-1} °C^{-1})	β_1	β_2	γ_1	γ_2
Sand	1.10×10^6	0.70	0.30	0.30	0.24	0.29	1.97	1.17
Glass beads	0.97×10^6	0.59	0.41	0.20	0.28	0.32	0.92	0.22

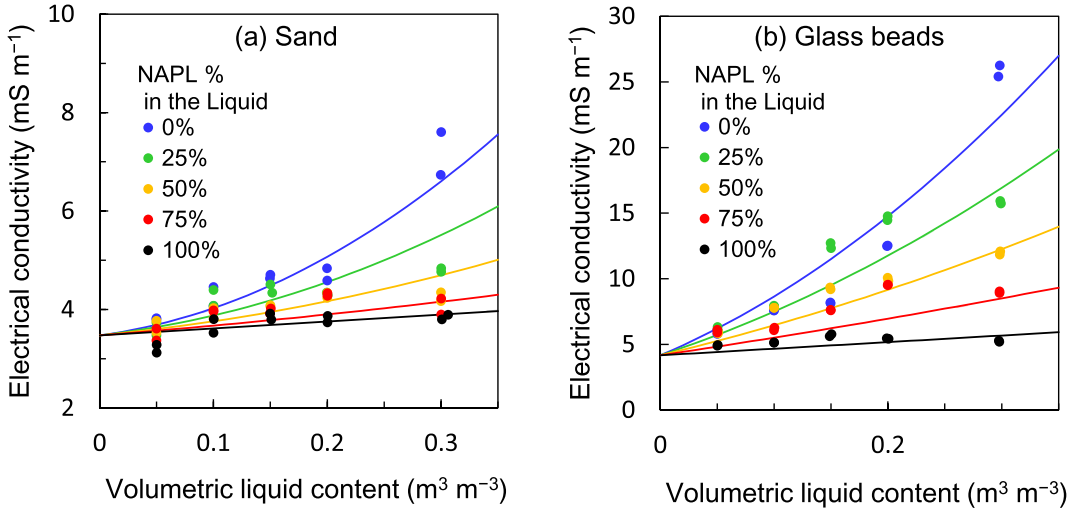

Fig. 2. The relationship between soil volumetric liquid content and bulk electrical conductivity. Points are the observations and solid curves are fits of Eq. (6) to data. Different colors represent different concentrations of non-aqueous phase liquid (NAPL) in the soil liquid.

Because NAPL is not soluble, in addition, there is a possibility that non-homogeneous distributions of NAPL in soil affected the measured σ_b values. The RMSE values for sand and glass beads were 0.3 mS m^{-1} and 1.6 mS m^{-1}, and MAPE values for sand and glass beads values were 5.6 % and 13.4 %. The MAPE value for glass beads was large in part because of the difficulty to obtain accurate σ_b measurements. The fitted σ_{NAPL} values relatively large, i.e., 1.28 mS m^{-1} and 2.01 mS m^{-1} for sand and glass beads. The actual electrical conductivity of Canola oil was reported to be smaller than 5.0×10^{-6} mS m^{-1} (Sankaran et al., 2019), so these numbers were products of data fitting and did not represent actual

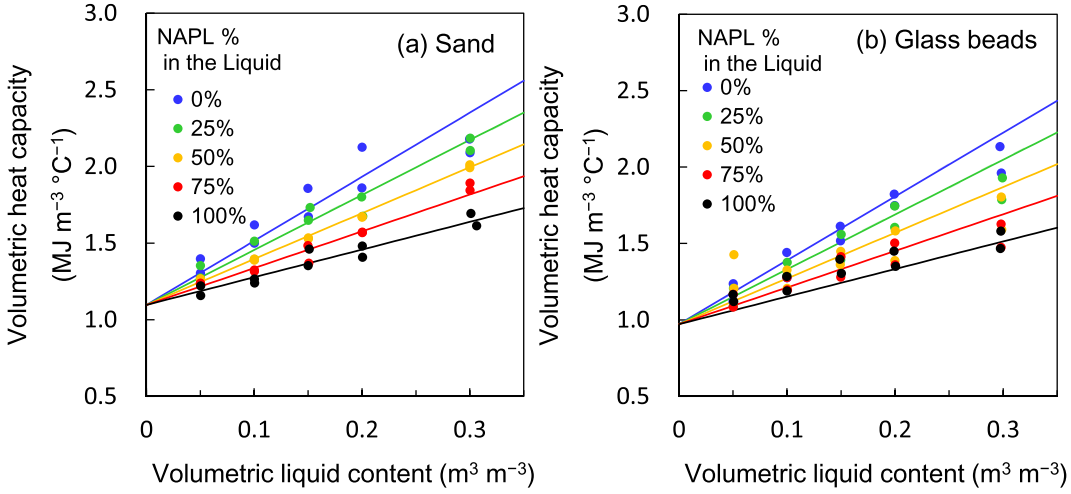

Fig. 3. The relationship between soil volumetric liquid content and volumetric heat capacity. Points are the observations and solid lines are fits of Eq. (7) to data. Different colors represent different concentrations of non-aqueous phase liquid (NAPL) in the soil liquid.

values. Because we assumed that NAPL intrusion altered water distribution in pores causing a change in σ_b, the relatively large σ_{NAPL} values indicated that they included the effect of water electrical conductivity.

Fig. 3 shows the relationship between θ_l and C. Increases in θ_l increased C, and the increases were larger at low solution concentrations. Unlike ε_b and σ_b, the trend of θ_l and C was linear, because C is proportional to the volume fraction of each soil constituent as expressed by Eq. (7). The C of sand increased from 1.4 MJ m^{-3} $°C^{-1}$ to 2.1 MJ m^{-3} $°C^{-1}$, and the C of glass beads increased from 1.2 MJ m^{-3} $°C^{-1}$ to 2.0 MJ m^{-3} $°C^{-1}$ as θ_l increased from 0.05 m^3 m^{-3} to 0.30 m^3 m^{-3} when NAPL concentration in the solution was zero. The C values of sand went from 1.2 MJ m^{-3} $°C^{-1}$ to 1.7 MJ m^{-3} $°C^{-1}$, and those of glass beads went from 1.1 MJ m^{-3} $°C^{-1}$ to 1.5 MJ m^{-3} $°C^{-1}$, when NAPL concentration was 100 %. Fig. 3 presents the fitted Eq. (7) values as solid lines, and the fitted parameters are shown in Table 1. The line slope is C_w for 0 % NAPL, and C_{NAPL} for 100 % NAPL. Although Eq. (7) described the relationships well, some points differed from the fitted lines. Rather than being actual differences associated with real phenomena such as inhomogeneous distribution of water and NAPL, the deviations were likely caused by small changes in probe spacing when the thermo-TDR sensor was inserted into a sample. Because C represented a sum of products of volumetric heat capacity and volume fraction of soil constituents, C was not influenced by how the constituents distributed in the sampling volume. We observed significant measurement errors in $\theta_l = 0.30$ m^3 m^{-3} sand, possibly due to a probe deflection. Because the $\theta_l = 0.30$ m^3 m^{-3} sand sample was packed relatively hard compared to the other samples, a change in probe spacing critical to C determination might have occurred when the probe was inserted into the sample. Other than the $\theta_l = 0.30$ m^3 m^{-3} sand, glass beads with a high NAPL concentration (>50 %) showed relatively large errors, which was also possibly due to a probe deflection. The RMSE and MAPE values were 0.07 MJ m^{-3} $°C^{-1}$ and 3.0 % for sand, and 0.11 MJ m^{-3} $°C^{-1}$ and 5.9 % for glass beads. The RMSE and MAPE values of glass beads were slightly larger than those of sand. This occurred because the errors were larger for glass beads than for sand in samples with high NAPL concentration (>50 %) as mentioned earlier.

The slopes of the $\lambda(\theta_l)$ curves were relatively large when θ_l was small, and the slopes decreased as θ_l increased (Fig. 4). This was because the liquid induced an increase in connectivity of soil particles when θ_l was small, and it was also observed when the liquid consisted only of NAPL. The λ of sand increased from 1.2 W m^{-1} $°C^{-1}$ to 2.2 W m^{-1} $°C^{-1}$, and the λ of glass beads increased from 0.4 W m^{-1} $°C^{-1}$ to 0.8 W m^{-1} $°C^{-1}$ as θ_l increased from 0.05 m^3 m^{-3} to 0.30 m^3 m^{-3} when NAPL concentration in the solution was zero. Related values for sand were from 0.6 W m^{-1} $°C^{-1}$ to 1.1 W m^{-1} $°C^{-1}$, and those of glass beads were from 0.3 W m^{-1} $°C^{-1}$ to 0.5 W m^{-1} $°C^{-1}$ when NAPL concentration was 100 %. The λ of sand was approximately twice that of glass beads. This was reasonable because the soil particles had the largest thermal conductivity among the soil constituents, and the larger particle size, the larger the thermal conductivity. The slopes in the $\lambda(\theta_l)$ curves decreased as NAPL concentration in the solution increased, because λ of NAPL was smaller than that of water, 0.17 W m^{-1} $°C^{-1}$ and 0.58 W m^{-1} $°C^{-1}$, respectively (Rojas et al., 2013; de Vries, 1963). The fitted Eqs. (8) and (9) are shown in Fig. 4 as solid curves, and the fitted parameters are shown in Table 1. Eqs. (8) and (9) captured the relationship between θ_l and λ quite well. The RMSE and MAPE values were 0.04 W m^{-1} $°C^{-1}$ and 2.3 % for sand, and 0.02 W m^{-1} $°C^{-1}$ and 3.1 % for glass beads. The MAPE of λ was the smallest among the four parameters. It indicated that the scattering of the measurement plot was slight, and the measurement accuracy was high. It was attributed to the fact that the λ measurements were independent of the probe spacing and were not affected by probe deflections.

3.2. Sensitivity analysis

The sensitivity analysis helps us to evaluate how sample water and NAPL contents affect electrical and thermal properties. Fig. 5 shows how φ of each soil property varies when both θ_w and θ_{NAPL} are 0.15 m^3 m^{-3}. The φ of sand ε_b to θ_w has a large value, 1.78, and those of other parameters are within a range of 0.27 to 0.33 (Fig. 5(a)). It indicates that ε_b varies more drastically than the other parameters at the same θ_w value. Thus, it is likely that θ_w can be estimated accurately from ε_b measurements. This is also supported by the large dielectric constants of water, 80, compared to those of other soil constituents, e.g., 3–10 for particles and 3.1 for Canola oil. This large difference resulted in the ε_b being more likely controlled by soil water content while NAPL effect faded in comparison. The other three parameters, σ_b, C, and λ, showed a similar degree of change for the θ_w value. The φ of sand properties to θ_{NAPL} were smaller than those for θ_w (Fig. 5(b)). The φ of ε_b for θ_w compared to θ_{NAPL} was significantly reduced from 1.78 to 0.23. The φ of sand ε_b, σ_b, and C to θ_{NAPL} were within a range of 0.14 to 0.23, but the φ of λ with θ_{NAPL} was small, i.e., 0.02. It indicates that λ was the least likely parameter to change as θ_{NAPL} changed. The φ values of glass beads with θ_w were similar to those of sand. The only difference was that the φ of σ_b increased from 0.33 to 0.75 (Fig. 5(c)). The increase of φ of σ_b occurred because the σ_b of glass beads was approximately-three times larger than that for sand (Fig. 2). Among the φ for θ_{NAPL} values, φ of electrical

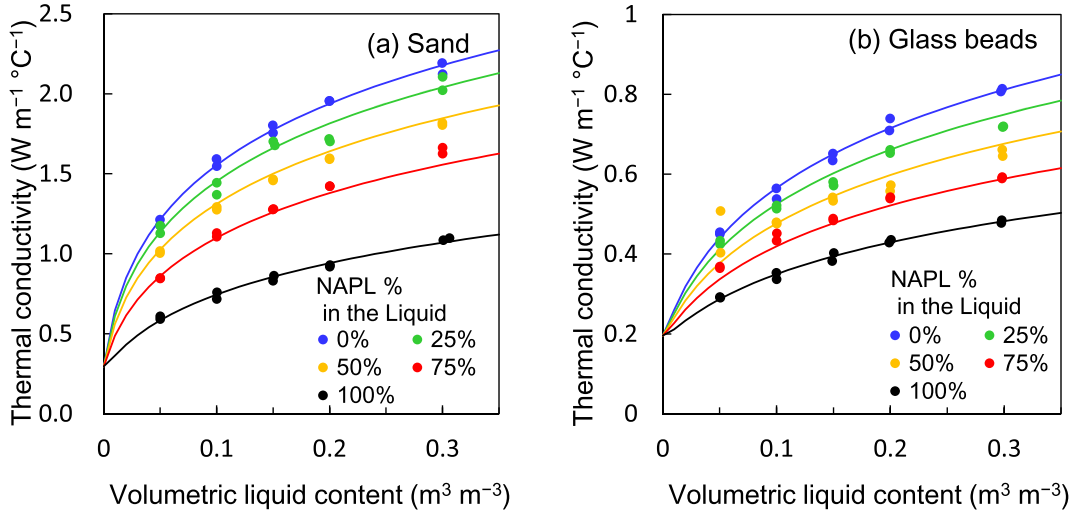

Fig. 4. The relationship between soil volumetric liquid content and thermal conductivity. Points are the observations and solid curves are fits of Eqs. (8) and (9) to data. Different colors represent different concentrations of non-aqueous phase liquid (NAPL) in the soil liquid.

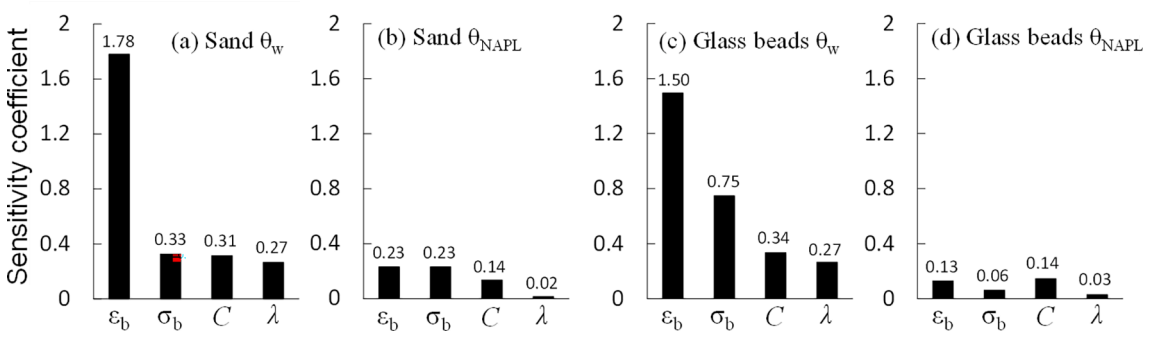

Fig. 5. Sensitivity coefficients of the soil bulk dielectric constant (ε_b), bulk electrical conductivity (σ_b), volumetric heat capacity (C), and thermal conductivity (λ) when soil water content (θ_w) and soil non-aqueous phase liquid content (θ_{NAPL}) each have a value of 0.15 m^3 m^{-3}. (a) Sensitivity coefficient of sand to θ_w, (b) Sensitivity coefficient of sand to θ_{NAPL}, (c) Sensitivity coefficient of glass beads to θ_w, and (d) Sensitivity coefficient of glass beads to θ_{NAPL}.

properties was smaller than those for sand, while the φ values of thermal properties were similar to those for sand. The glass beads φ values tended to be significant for the properties that depended on the volume fraction of constituents, i.e., ε_b and C, and to be small for the properties that depended on the connectivity of constituents, i.e., σ_b and λ. In both materials, sensitivities to θ_w were more significant than those to θ_{NAPL} for all parameters. This indicated that the four parameters were more affected by changes in θ_w than by changes in θ_{NAPL}.

Fig. 6 presents φ of the glass beads as a function of θ_w and θ_{NAPL} in contour plots. The φ values increased as θ_w increased, and the φ values increased as θ_{NAPL} increased. While the φ to θ_w was little affected by θ_{NAPL}, the φ to θ_{NAPL} was affected by changes in θ_w, i.e., φ to θ_{NAPL} increased as θ_w decreased. Only the φ of λ showed a notable trend. The φ of λ to θ_w increased as θ_{NAPL} decreased, and the φ of λ to θ_{NAPL} increased as θ_w decreased. The φ of λ to θ_{NAPL} were generally small, but they showed relatively large values (0.26–0.30) when θ_w was zero. The NAPL connected the soil particles, i.e., built bridges, and controlled λ when there was no water, but such a role was taken away by the water even with a small amount of water present. Sand showed a similar trend, albeit with different values (data not shown). The sensitivities of the four properties to water and NAPL in soil were revealed. The parameters best suited for θ_w and θ_{NAPL} determinations might be determined overall from sensor measurement accuracy and sensitivity strength.

3.3. Estimation of soil water and NAPL content

Three different approaches were tested to estimate θ_w and θ_{NAPL} from the thermo-TDR measurements. Fig. 7 shows the θ_w and θ_{NAPL} values estimated by the first (ε_b & C-based) approach. The θ_w of sand was accurately estimated with this approach, although there were slight overestimations when θ_w was small, i.e., a range of 0 to 0.05 m^3 m^{-3} (Fig. 7(a)). The first approach determined θ_w directly from ε_b and C values with Eq. (13), so that the measurement errors in the two parameters led to the errors in θ_w. The sand θ_{NAPL} estimations showed a scattering of data points (Fig. 7(b)). When the NAPL concentration in the soil solution was large, such as 75 % and 100 % (red and black points in the figures), the estimated θ_{NAPL} values were similar to the reference values (close to the 1:1 line), and θ_{NAPL} was found to be estimated accurately. However, θ_{NAPL} values were overestimated as the NAPL concentration decreased. When the reference θ_{NAPL} value was zero, this approach sometimes gave a θ_{NAPL} value larger than 0.40 m^3 m^{-3}. As with θ_w, the θ_{NAPL} value was calculated directly from the measured values of ε_b and C with this approach. Thus, the measurement errors were included in the estimated θ_{NAPL} value. In addition, as shown from

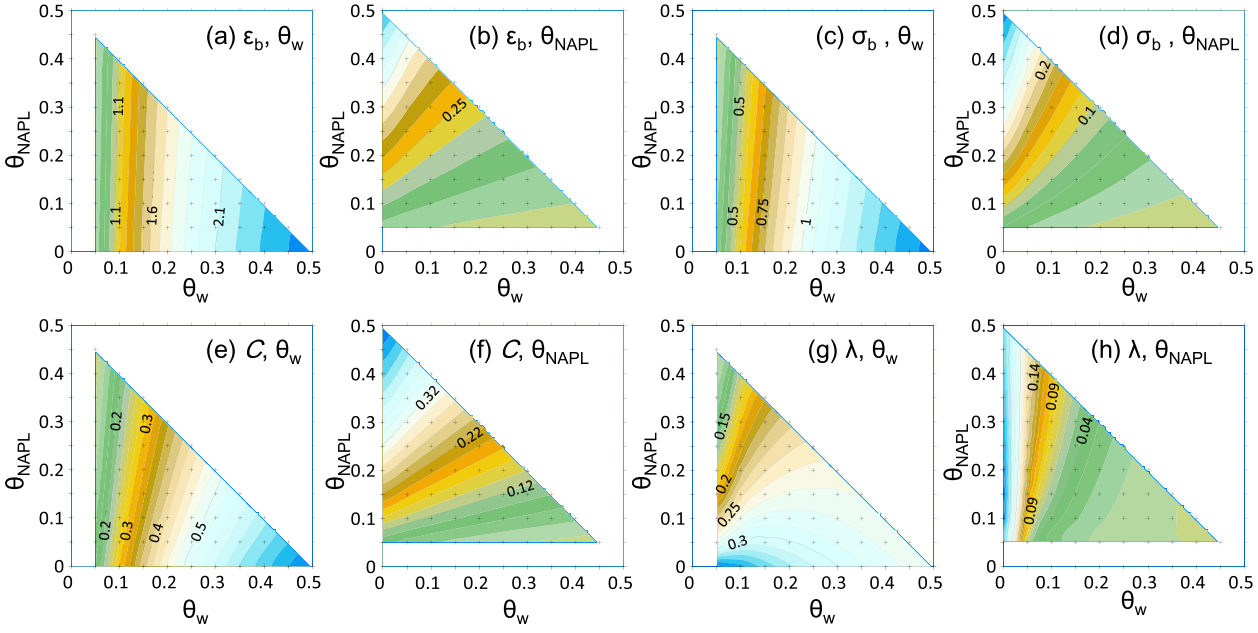

Fig. 6. Contours are presented of the glass beads sensitivity coefficients of soil bulk dielectric constant (ε_b), bulk electrical conductivity (σ_b), volumetric heat capacity (C), and thermal conductivity (λ) to soil water content (θ_w) (panels (a), (c), (e), and (g)) and soil non-aqueous phase liquid content (θ_{NAPL}) (panels (b), (d), (f), and (h)).

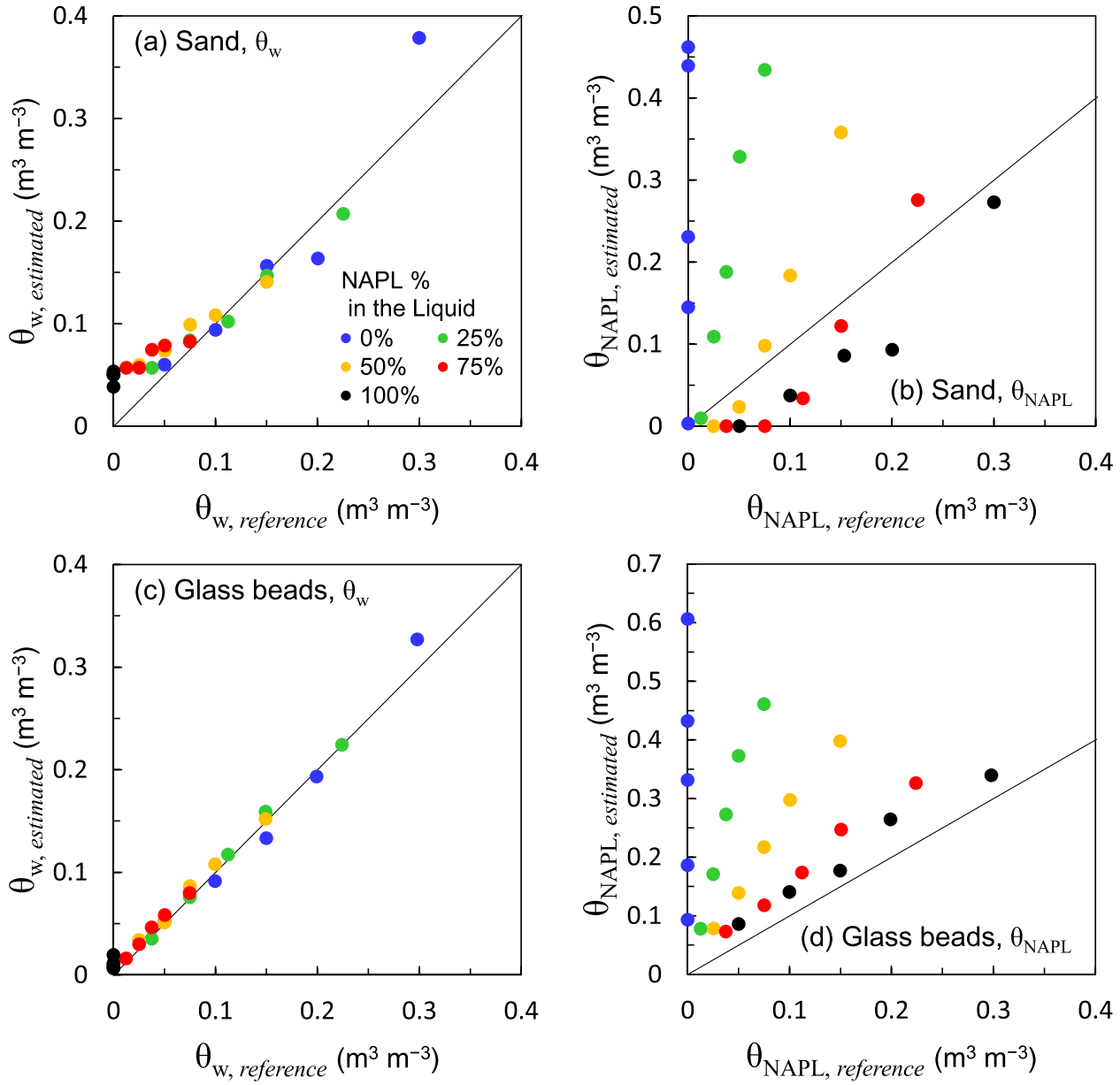

Fig. 7. Soil volumetric water content (θ_w) or volumetric non-aqueous phase liquid content (θ_{NAPL}) estimated with the soil bulk dielectric constant and volumetric heat capacity-based approach are compared to the reference values. The subscripts of *estimated* and *reference* indicate estimated and reference values of θ_w or θ_{NAPL}. Different colors represent different concentrations of non-aqueous phase liquid (NAPL) in the soil liquid. Panels (a) and (b) present results for sand, and panels (c) and (d) present results for glass beads.

the sensitivity analysis, the sensitivity of ε_b and C to θ_{NAPL} decreased as θ_w increased, so θ_{NAPL} estimation accuracy decreased as the NAPL concentration decreased. The RMSE values of the θ_w and θ_{NAPL} estimations were 0.034 $m^3\ m^{-3}$ and 0.180 $m^3\ m^{-3}$. The θ_w values of glass beads were estimated more accurately than those for sand (Fig. 7(c)). Overestimations of θ_w at small θ_w values were not observed. The θ_{NAPL} values of the glass beads were close to a 1:1 line when the NAPL concentrations were 75 % and 100 %, indicating that the estimated θ_{NAPL} values were accurate (Fig. 7(c)). Meanwhile, θ_{NAPL} was highly overestimated when NAPL concentrations were smaller than 75 %. A possible reason for this phenomenon was similar to that discussed for the sand, i.e., the effect of estimation errors in θ_w on θ_{NAPL} estimation got stronger as NAPL concentration decreased, because of a decrease in the sensitivities of both ε_b and C to θ_{NAPL}. The RMSE values for θ_w and θ_{NAPL} estimations in glass beads were 0.010 $m^3\ m^{-3}$ and 0.220 $m^3\ m^{-3}$. The good estimates of θ_w were due in part to the accurate glass beads ε_b values. The ε_b & C-based approach effectively determined large θ_{NAPL} values, while it overestimated θ_{NAPL} when actual θ_{NAPL} values were relatively small.

The θ_w and θ_{NAPL} values estimated with the second (ε_b & λ-based) approach are presented in Fig. 8. For both sand and glass beads, estimated θ_w values plotted near to the 1:1 line, indicating that the second approach provided accurate estimates (Fig. 8(a) and (c)). The estimated θ_{NAPL} values for both sand and glass beads were distributed between 0 $m^3\ m^{-3}$ to 0.15 $m^3\ m^{-3}$, and there was no clear correlation between the estimated values and the reference values (Fig. 8(b) and (d)). The limited sensitivity of λ to θ_{NAPL} might have caused inaccurate determinations of θ_{NAPL} (Fig. 5). Although the measurement errors in λ were small (Fig. 4), the λ values did not contribute much to the determination of θ_{NAPL}. The θ_w values were accurately estimated from ε_b and λ, because both were sensitive to θ_w. The ε_b & λ-based approach was not suitable for θ_{NAPL} determination. The RMSE values of θ_w and θ_{NAPL} estimations were 0.017 $m^3\ m^{-3}$ and 0.078 $m^3\ m^{-3}$ for sand, and 0.011 m^3

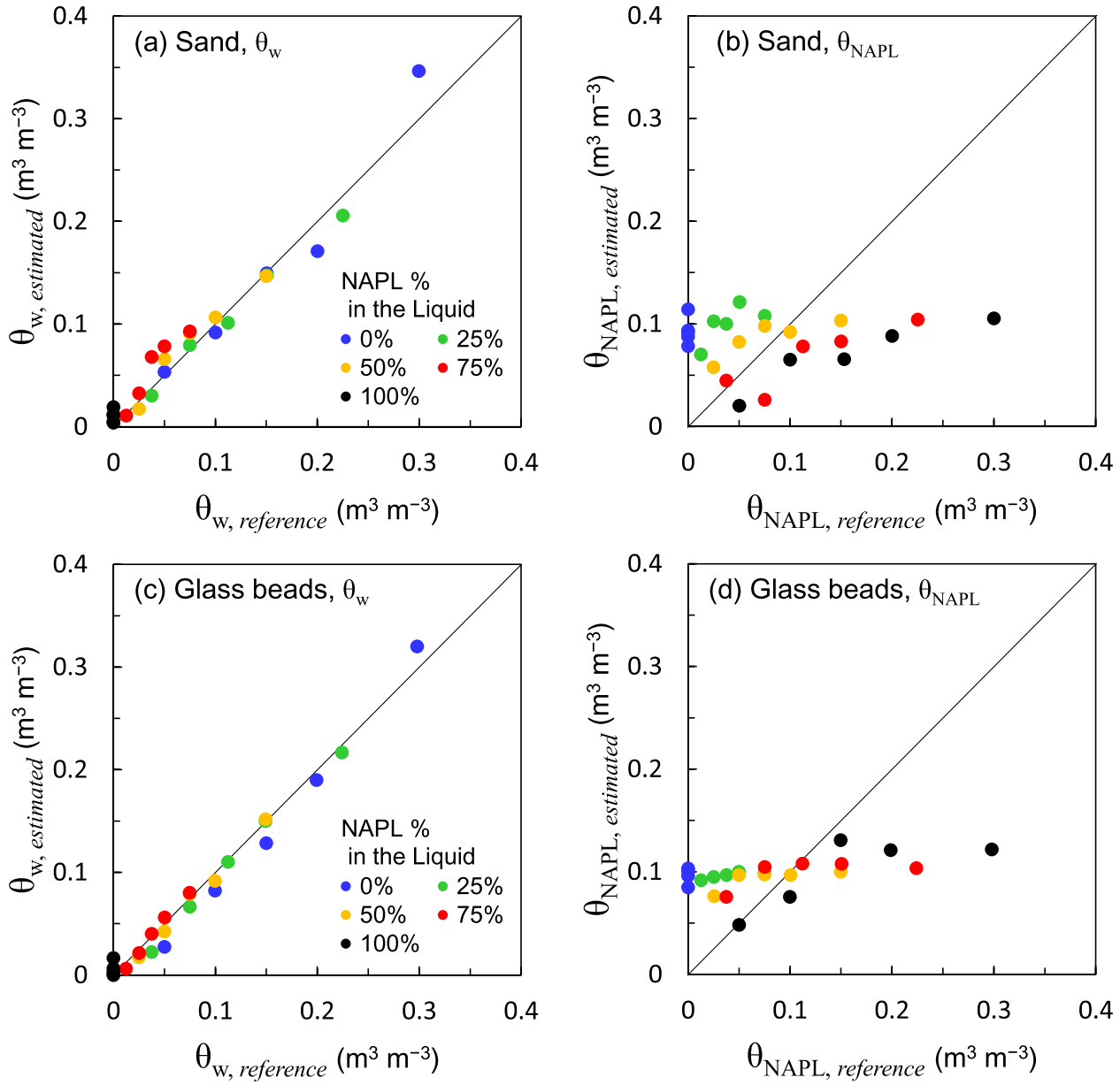

Fig. 8. Soil volumetric water content (θ_w) or volumetric non-aqueous phase liquid content (θ_{NAPL}) estimated with the soil bulk dielectric constant and thermal conductivity-based approach are compared to the reference values. The subscripts of *estimated* and *reference* indicate estimated and reference values of θ_w or θ_{NAPL}. Different colors represent different concentrations of non-aqueous phase liquid (NAPL) in the soil liquid. Panels (a) and (b) present results for sand, and panels (c) and (d) present results for glass beads.

m^{-3} and 0.072 m^3 m^{-3} for glass beads. The RMSE values became smaller than those with the ε_b & *C*-based approach because large over-estimations of θ_{NAPL} observed in Fig. 7 did not occurred.

The θ_w and θ_{NAPL} values estimated by the third (four-parameter-based) approach are shown in Fig. 9. The θ_w values of sand did not differ much from the initial values calculated with Eq. (13) (Fig. 9(a) and (c)), indicating that the four-parameter-based approach accurately estimated θ_w. The RMSE values of the θ_w estimations were 0.029 m^3 m^{-3} and 0.011 m^3 m^{-3} for sand and glass beads, similar to the RMSEs of the ε_b & *C*-based approach. The four-parameter-based approach provided better θ_{NAPL} estimations than those from the first and second approaches. While some points converged to zero as a result of optimization, most points were distributed near the 1:1 line (Fig. 9(b), (d)). For reference values smaller than 0.1 m^3 m^{-3} some of the sand estimates converged to zero, but the glass beads estimates and the sand estimates larger than 0.1 m^3 m^{-3} were consistent with the reference values. In particular, the glass beads θ_{NAPL} estimates were quite accurate. A significant over-estimation at a reference θ_{NAPL} value of zero occurred for one sand value of $\theta_{NAPL} = 0.198$ m^3 m^{-3}. This was a significant improvement over the ε_b & *C*-based estimates. The RMSE values of θ_{NAPL} estimations were 0.066 m^3 m^{-3} and 0.042 m^3 m^{-3}, which were the smallest values among the three approaches. Compared to the ε_b & *C*-based approach, the four-parameter-based approach estimated θ_{NAPL} indirectly, averaging out the effects of measurement errors in each parameter. Thus, the accuracy was greatest for θ_{NAPL} estimations with the four-parameter-based approach.

The estimation accuracy of θ_{NAPL} was better for glass beads than for sand. It might be due to a pore size effect, because NAPL was insoluble, water and NAPL existed separately in soil pores. Although an effort was made to pack samples with uniform water and NAPL distributions, internal movement might have occurred during measurements, resulting in non-uniform distributions in the samples. Such a phenomenon could

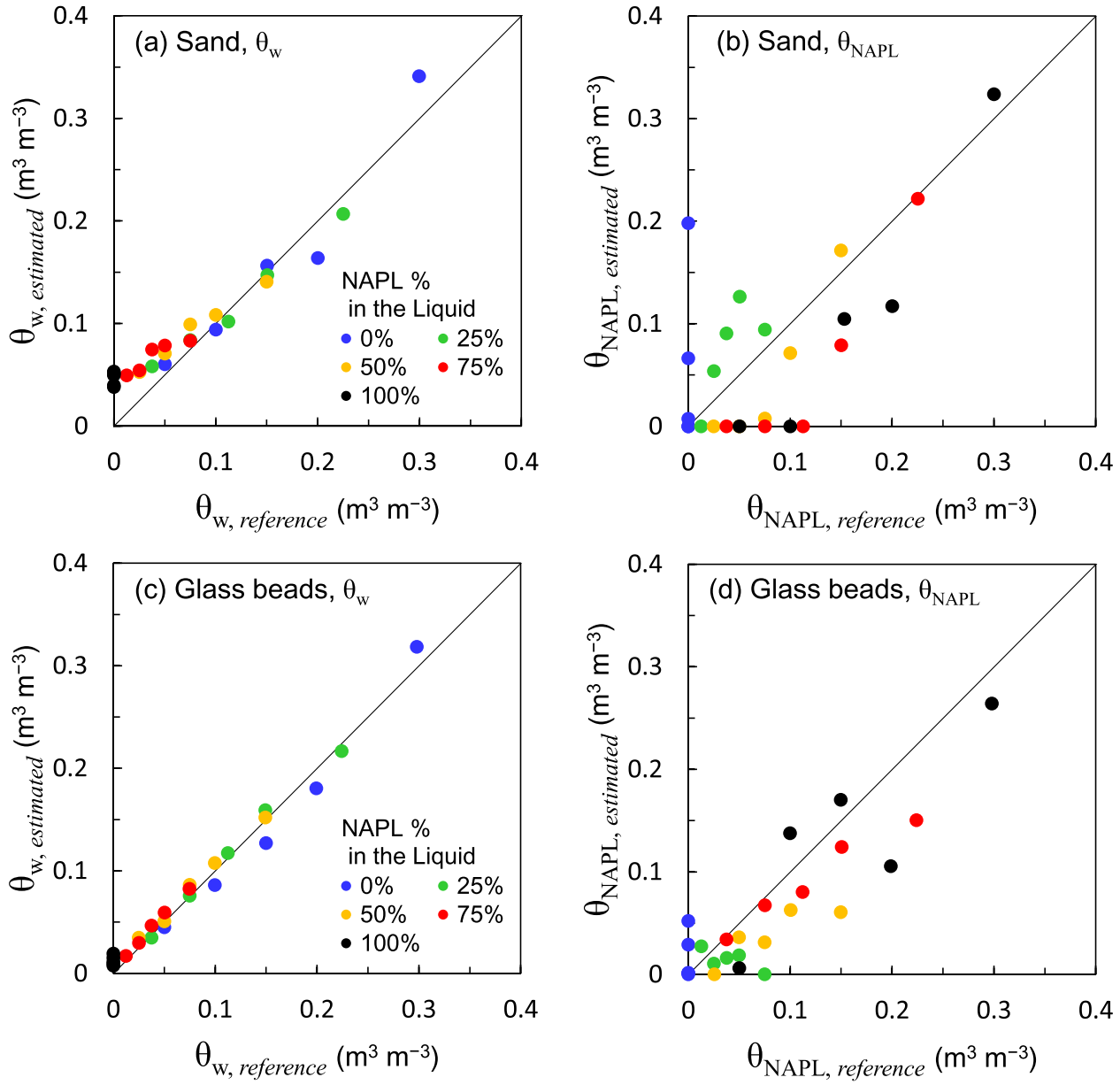

Fig. 9. Soil volumetric water content (θ_w) or volumetric non-aqueous phase liquid content (θ_{NAPL}) estimated with the four-parameter-based approach are compared to the reference values. The subscripts of *estimated* and *reference* indicate estimated and reference values of θ_w or θ_{NAPL}. Different colors represent different concentrations of non-aqueous phase liquid (NAPL) in the soil liquid. Panels (a) and (b) present results for sand, and panels (c) and (d) present results for glass beads.

more readily manifest in the sand, which had larger pore sizes than the glass beads. While the four-parameter-based approach provided relatively accurate estimates of θ_{NAPL}, a challenge remained to accurately estimate small θ_{NAPL} values in coarse soils. Future research should investigate the use of additional thermo-TDR sensor designs like that of Peng et al. (2019), which might be able to increase the measurement accuracy of each parameter and improve the accuracy of θ_{NAPL} estimations. Although this study investigated Canola oil as a NAPL, slightly different results are expected for other NAPL compounds, so future investigations are encouraged.

4. Conclusions

We focused on the use of a thermo-TDR sensor as a tool to estimate in-situ NAPL content in variably-saturated contaminated soil and established a relationship between four thermo-TDR soil properties (ε_b, σ_b, C, and λ) and water and NAPL contents. Our newly established relationship was expressed via conventional or new models, and the sensitivity of each soil property to θ_w and θ_{NAPL} was evaluated based on the models. Furthermore, we proposed and evaluated three different approaches to estimate θ_{NAPL} values from thermo-TDR measured soil parameters, i.e., the ε_b & C-based, the ε_b & λ-based, and the four-parameter-based approaches. A sensitivity analysis revealed that θ_w rather than θ_{NAPL} dominated all four thermo-TDR parameters. The sensitivity of the four parameters to θ_{NAPL} varied among the samples. The sensitivities of electrical properties were more significant than those of thermal properties for sand. The sensitivities of volume-based properties, ε_b and C, were more extensive than those of connectivity-based properties, σ_b and λ, for glass beads. The ε_b & C-based approach to estimate θ_{NAPL} values, which calculated θ_{NAPL} values directly from ε_b and C, was susceptible to measurement errors, and the ε_b & λ-based approach failed to estimate the θ_{NAPL} because of the small sensitivity of λ to θ_{NAPL}. For the four-parameter-based approach the effects of measurement errors were suppressed by the optimization process, which allowed the

more highly sensitive parameters to cover for the lower sensitivity parameters. Thus, the four-parameter-based approach provided the most accurate estimations of θ_{NAPL}. Use of the thermo-TDR sensor to determine θ_{NAPL} values should contribute to future NAPL contamination studies in soil.

5. Author statement

Yuki Kojima, drafting the manuscript, conception, design of the study, and data analysis; Kenta Okumura, data acquisition; Shinsuke Aoki, conception and design of the study; Kosuke Noborio, conception and design of the study; Kohji Kamiya, conception and design of the study; Robert Horton, conception and design of the study, revising manuscript critically for important intellectual content.

Declaration of Competing Interest

The authors declare that they have no known competing financial interests or personal relationships that could have appeared to influence the work reported in this paper.

Data availability

Data will be made available on request.

Acknowledgments

This work was supported by Grants-in-Aid for Early-Career Scientist 21K14940 from Japan Society for the Promotion of Science, Koshiyama Research Grants for Science and Technology, the US National Science Foundation (Grant Number: 2037504) and USDA-NIFA Multi-State Project 4188.

References

Ajo-Franklin, J.B., Geller, J.T., Harris, J.M., 2004. The dielectric properties of granular media saturated with DNAPL/water mixtures. Geophys. Res. Lett. 31, L17501.

Aoki, S., Noborio, K., 2019. Simultaneous water and oil contents measurements with thermo-time domain reflectometry. In SSSA International Soils Meeting, Jan. 6-9, 2019, San Diego, CA.ASA-CSSA-SSSA. https://scisoc.confex.com/scisoc/2019sssa/meetingapp.cgi/Paper/115606.

Birchak, J.R., Gardner, C.G., Hipp, J.E., Victor, J.M., 1974. High dielectric constant microwave probes for sensing soil moisture. Proc. IEEE 62, 93–98.

Bristrow, K.L., Kluitenberg, G.J., Horton, R., 1994. Measurement of soil thermal properties with a dual-probe heat-pulse technique. Soil Sci. Soc. Am. J. 58, 1288–1294.

Campbell, G.S., Calissendorff, C., Williams, J.H., 1991. Probe for measuring soil specific heat using a heat-pulse method. Soil Sci. Soc. Am. J. 55, 291–293.

Comegna, A., Coppola, A., Dragonetti, G., Sommella, A., 2016. Estimating nonaqueous-phase liquid content in variably saturated soils using time domain reflectometry. Vadose Zone J. 15 (5) https://doi.org/10.2136/vzj2015.11.0145.

Comegna, A., Coppola, A., Dragonetti, G., Severino, G., Sommella, A., 2018. Interpreting TDR signal propagation through soils with distinct layers of nonaqueous-phase liquid and water content. Vadose Zone J. 16 (13) https://doi.org/10.2136/vzj2017.07.0141.

Comegna, A., Coppola, A., Dragonetti, G., Sommella, A., 2019. A soil non-aqueous phase liquid (NAPL) flushing laboratory experiment based on measuring the dielectric properties of soil-organic mixtures via time domain reflectometry (TDR). Hydrol. Earth Syst. Sci. 23, 3593–3602.

de Vries, D.A., 1963. Thermal properties of soils. In: van Wijk, W.R. (Ed.), Physics of Plant Environment. North-Holland Publ, Amsterdam, pp. 210–235.

Dobson, M.C., Ulaby, F.T., Hallikainen, M.T., El-Rayes, M.A., 1985. Microwave dielectric behavior of wet soil, part II: dielectric mixing models. IEEE Trans. Geosci. Remote Sens. GE-23(1), 35–46.

Francisca, F.M., Montoro, M.A., 2012. Measuring the dielectric properties of soil-organic mixtures using coaxial impedance dielectric reflectometry. J. Appl. Geophys. 80, 101–109.

Frederikse, H.P.R., 2009. Permittivity (dielectric constant) of inorganic solids. In: Lide, D.R. (Ed.), CRC Handbook of Chemistry and Physics, 90th Edition, CRC Press, Boca Raton, pp. 210-235. pp.12–47-12–58.

Haridy, S.A., Persson, M., Berndtsson, R., 2004. Estimation of LNAPL saturation in fine sand using time-domain reflectometry. Hydrolog. Sci. J. 49 (6), 987–1000.

He, H., Dyck, M.F., Horton, R., Ren, T., Bristow, K.L., Lv, J., Si, B., 2018. Development and application of the heat pulse method for soil physical measurements. Rev. Geophys. 56, 567–620.

Ju, Z., Sun, H., Liu, X., 2020. Thermo-time domain reflectometry to evaluate unsaturated soils contaminated with non-aqueous phase liquids. Vadose Zone J. 19, e20016.

Kojima, Y., Heitman, J.L., Noborio, K., Ren, T., Horton, R., 2018. Sensitivity analysis of temperature changes for determining thermal properties of partially frozen soil with a dual probe heat pulse sensor. Cold Reg. Sci. Technol. 151, 188–195.

Leharne, S., 2019. Transfer phenomena and interactions of non-aqueous phase liquids in soil and groundwater. ChemTexts 5, 5.

Lizhi, H., Toyoda, K., Ihara, I., 2008. Dielectric properties of edible oils and fatty acids as a function of frequency, temperature, moisture and composition. J. Food Eng. 88, 151–158.

Lu, Y., Lu, S., Horton, R., Ren, T., 2014. An empirical model for estimating soil thermal conductivity from texture, water content, and bulk density. Soil Sci. Soc. Am. J. 78, 1859–1868.

McCray, J.E., Falta, R.W., 1997. Numerical simulation of air sparging for remediation of NAPL contamination. Ground Water 35 (1), 99–110.

Mochizuki, H., Koiwasaki, M., Suko, T., 2007. Thermal conductivity of washed tottori dune sand with rape seed oil and modeling. (in Japanese with English abstract). J. Jpn. So. Soil Phys. 105, 59–65.

Mohamed, A.M.O., Said, R.A., 2004. TDR detection of non-aqueous phase liquid in sandy soils using the eigendecomposition method. Environ. Geol. 47, 30–37.

Mohamed, A.M.O., Said, R.A., 2005. Detection of organic pollutants in sandy soils via TDR and eigendecomposition. J. Contam. Hydrol. 76, 235–249.

Moroizumi, T., Hanzawa, W., Sasaki, C., 2008. Estimation of NAPL content in saturated sandy soil using dual-probe heat-pulse method (in Japanese with English abstract). J. Groundwater Hydrol. 50 (1), 17–24.

Moroizumi, T., Sasaki, Y., 2008. Estimating the nonaqueous-phase liquid content in saturated sandy soil using amplitude domain reflectometry. Soil Sci. Soc. Am. J. 72 (6), 1520–1526.

Noborio, K., 2001. Measurement of soil water content and electrical conductivity by time domain reflectometry: a review. Comput. Electron. Agr. 31, 213–237.

Noborio, K., 2005. Measuring concentration of organic contaminants in unsaturated soil with a thermo-time domain reflectometry probe. (in Japanese with English abstract). J. Jpn. Soc. Civil Eng. 783, 33–38.

Noborio, K., 2013. Sensors for measuring soil environment (in Japanese). J. Soc. Inst. Control Eng. 52 (8), 672–678.

Noborio, K., McInnes, K.J., Heilman, J.L., 1996. Measurements of soil water content, heat capacity, and thermal conductivity with a single TDR probe. Soil Sci. 161 (1), 22–28.

Peng, W., Lu, Y., Xie, X., Ren, T., Horton, R., 2019. An improved thermo-TDR technique for monitoring soil thermal properties, water content, bulk density, and porosity. Vadose Zone J. 18, 190026 https://doi.org/10.2136/vzj2019.03.0026.

Persson, M., Berndtsson, R., 2002. Measuring non-aqueous phase liquid saturation in soil using time domain reflectometry. Water Resour. Res. 38 (5), 1064.

Regalado, C.M., Carpena, M., Socorro, A.R., Hernández Moreno, J.M., 2003. Time domain reflectometry models as a tool to understand the dielectric response of volcanic soils. Geoderma 117, 313–330.

Ren, T., Noborio, K., Horton, R., 1999. Measuring soil water content, electrical conductivity, and thermal properties with a thermo-time domain reflectometry probe. Soil Sci. Soc. Am. J. 63, 450–457.

Rhoades, J.D., Raats, P.A.C., Prather, R.J., 1976. Effects of liquid-phase electrical conductivity, water content, and surface conductivity on bulk soil electrical conductivity. Soil Sci. Soc. Am. J. 40, 651–655.

Rinaldi, V.A., Francisca, F.M., 2006. Removal of immiscible contaminants from sandy soils monitored by means of dielectric measurements. J. Environ. Eng. 132 (8), 931–939.

Robinson, D.A., Jones, S.B., Wraith, J.M., Or, D., Friedman, S.P., 2002. A review of advances in dielectric and electrical conductivity measurement in soils using time domain reflectometry. Vadose Zone J. 2, 444–475.

Rojas, E.E.G., Coimbra, J.S.R., Telis-Romero, J., 2013. Thermophysical properties of cotton, canola, sunflower and soybean oils as a function of temperature. Int. J. Food Prop. 16 (7), 1620–1629.

Sankaran, A., Staszel, C., Belknap, D., Yarin, A.L., Mashayek, F., 2019. Effect of atmospheric humidity on electrical conductivity of oil and implications in electrostatic atomization. Fuel 253, 283–292.

Soga, K., Page, J.W.E., Illangasekare, T.H., 2004. A review of NAPL source zone remediation efficiency and the mass flux approach. J. Hazard. Mater. 110, 13–27.

Topp, G.C., Davis, J.L., Annan, A.P., 1980. Electromagnetic determination of soil water content: measurements in coaxial transmission lines. Water Resour. Res. 16 (3), 574–582.

Yilmaz, I., Kaynar, O., 2011. Multiple regression, ANN (RBF, MLP) and ANFIS models for prediction of swell potential of clayey soils. Expert Syst. Appl. 38, 5958–5966.